

Article

# Direct Membrane Filtration for Wastewater Treatment Using an Intermittent Rotating Hollow Fiber Module

Ignacio Ruigómez , Enrique González , Luis Rodríguez-Gómez and Luisa Vera \*

Departamento de Ingeniería Química y Tecnología Farmacéutica, Universidad de La Laguna (ULL), Facultad de Ciencias—Sección de Química, Avenida Astrofísico Francisco Sánchez, s/n. Campus de Anchieta, Apdo. de Correos 456, CP 38200 La Laguna, Tenerife, Spain; isempere@ull.es (I.R.); eglezc@ull.es (E.G.); luerguez@ull.es (L.R.-G.)

\* Correspondence: luvera@ull.edu.es; Tel.: +34-922-318-054

Received: 8 June 2020; Accepted: 24 June 2020; Published: 26 June 2020



**Abstract:** Direct membrane filtration of municipal wastewater has attracted a considerable interest in recent years. Preventing severe membrane fouling is a crucial issue in the process development. This paper aims to assess the effectiveness of a rotating hollow fiber module in enhancing fouling control. The effect of rotation speed, intermittence and permeate flux was studied in short-term tests at lab-scale. A combined filtration model considering residual fouling, intermediate pore blocking and cake filtration was used to analyze the effect of the shear induced by rotation. Results showed a significant flux improvement by increasing rotation shear stress and showed a nearly linear correlation between the threshold flux (ranged between 12 and 32 L·h<sup>-1</sup>·m<sup>-2</sup>) and the rotation speed. A proper rotation intermittence (10/15 on/off) was found, which may maintain a fouling control comparable to that achieved for continuous rotation. For a given energy demand, the optimal operating conditions involve high speeds ( $\geq 180$  rev·min<sup>-1</sup>) with low to moderate intermittences. Analyzing the relative contribution of the different feedwater fractions on membrane fouling, colloidal particles and macromolecules were found to be the main contributors.

**Keywords:** ultrafiltration; mechanical shear; threshold flux; fouling; shear-enhanced filtration

## 1. Introduction

In the last decades, population growth, pollution, urbanization and climate change are beginning to overwhelm nature's ability to provide freshwater resources. In order to reverse this situation and achieve water sustainability, wastewater treatment and reuse must be further developed and implemented [1]. It is also expected that the transition to a circular economy should create significant synergies for enhancing this implementation [2]. There is large experience in arid or semi-arid regions, where the reuse of treated wastewater has been recognized as a sustainable and cost-effective water resource [3,4]. Globally, agriculture irrigation is the largest consumer, accounting for 32% of the reclaimed wastewater, followed by landscape irrigation (20%) and industrial uses (19%) [5].

The selection of a treatment train or scheme for wastewater reclamation and reuse depends on several factors including the wastewater type, available area, cost, population size, social acceptance and level of quality to be reached [6]. Nevertheless, and regardless of the different factors, membrane-based technologies play an essential role since they provide better assurance of treatment for safe applications. One emerging membrane technology is direct membrane filtration (DMF) of raw wastewater [7,8]. By using a micro/ultrafiltration membrane, solids and pathogens can be removed from wastewater producing a readily reclaimed wastewater for irrigation and landscaping. In terms of chemical oxygen demand, removal efficiencies for municipal wastewaters in the range between 45% and 90% have been reported, according to membrane and wastewater characteristics [9–11]. Several advantages over

other comparative technologies (e.g., activated sludge followed by micro/ultrafiltration or membrane bioreactor) have been described: lower energy consumption, smaller footprint and higher nutrient content of the reclaimed wastewater. In addition, the rejected stream, rich in organic matter, can be anaerobically digested in order to produce biogas suitable for cogeneration of heat and power.

The main concern of DMF is the severe membrane fouling issue, which leads to lower operating fluxes and higher cleaning frequency than other membrane technologies. This fouling potential has been related to the large content of colloidal and soluble organic matter in the wastewater [7], which is not removed by biological pretreatment. In addition, under conditions of high substrate and low dissolved oxygen levels, stressed microorganisms can secrete extracellular polymeric substances, which have been identified as main foulants [12]. In addition, recent studies have also pointed out that wastewater cations, such as calcium or magnesium, can promote the abiotic aggregation of dissolved polysaccharides resulting in transparent exopolymer particles (TEP). Although there is no clear consensus on the role that TEP plays during wastewater ultrafiltration, it seems that these particles could contribute to foul the membranes via gel layer or protobiofilm formation, favoring the deposition of microorganisms on the membrane surface [13,14]. For the submerged membrane configuration, which is less energy intensive than the sidestream configuration [15], traditional physical methods have been applied to prevent membrane fouling, including continuous or intermittent air/gas sparging and backwashing. Diamantis et al. [16] have compared the performance of submerged flat sheet membranes with air sparging when filtering different feedwaters. They observed that fluxes for raw wastewater were significantly lower ( $7 \text{ L}\cdot\text{h}^{-1}\cdot\text{m}^{-2}$ ) than those obtained for secondary effluents ( $29 \text{ L}\cdot\text{h}^{-1}\cdot\text{m}^{-2}$ ). A flux of  $10 \text{ L}\cdot\text{h}^{-1}\cdot\text{m}^{-2}$  has been also reported for submerged hollow-fiber modules with gas sparging [9]. In addition, regular in situ chemical cleanings have to be adopted (every 6–48 h of filtration) for achieving a sustainable operation, in detriment of membrane lifespan. Therefore, due to the serious membrane fouling associated with DMF of raw wastewater, significant total costs (capital and operational) have been estimated [16].

To limit the fouling impact and also with the aim of increasing the organic removal efficiency, several pre-treatments such as coagulation, adsorption or ozonation have been applied [7]. In general, the studies highlight an improvement of process performance by the addition of inorganic coagulants, which has been attributed to the aggregation of fine particles and colloids into larger flocs, that tended to form a reversible cake layer on the membrane, thus enhancing physical cleaning efficiency [17–19]. A further improvement of this treatment has been reported by incorporating powdered activated carbon [20]. Nevertheless, coagulants dose can be high depending on the type of wastewater. Given the variability of composition of the wastewater (together with the ambient conditions), conducting the operation at an optimal dose can be a complex issue and it has been reported that large dosages of coagulant can induce a sharp increase of membrane fouling [21]. Furthermore, the addition of inorganic coagulant affects permeate quality [22] and also generates a concentrated stream with a relative high concentration of chemicals, which may have an environmental impact.

In this scenario, dynamic filtration systems, which create shear rates in the vicinity of the membrane surface by a moving part, offer an alternative fouling control strategy for DMF. Most established systems are based on membrane disks (rotating and vibrating) and hollow-fiber modules (vibrating) [23]. These systems have demonstrated their superior fouling control ability in challenging feedwaters [24]. In fact, previous studies have applied vibrating membranes in DMF, showing a better fouling control than air sparging [25,26]. Based on this approach, a novel rotating hollow-fiber module was applied for filtering raw wastewater, showing a performance comparable to that obtained for a pre-coagulated wastewater [27]. Nevertheless, the application of a fixed rotation speed in the module becomes energy intensive, while intermittent rotation seems to be energy-effective to prevent membrane fouling. Therefore, this paper aims to explore the effectiveness in enhancing fouling control of an intermittent rotating module applied to raw wastewater treatment. The membrane performance was evaluated at different flux conditions. For a deeper analysis of the fouling mechanisms and their relationship with

the main wastewater fractions, a combined filtration model considering residual fouling, intermediate pore blocking and cake filtration has been proposed.

## 2. Materials and Methods

### 2.1. Feedwater

The experimental unit was fed with screened, degrittied, degreased and sieved domestic wastewater from the wastewater treatment plant of Noreste (Canary Islands, Spain). The feedwater was characterized once per week during the experimental period. Table 1 summarizes the average values of main parameters. As seen, the feedwater can be considered as a high concentrated wastewater, with a large fraction of particulate matter.

**Table 1.** Average values of main characteristics of feedwater.

Parameter	Units	Mean	Standard Deviation
COD	mg·L <sup>-1</sup>	1073	160.3
DOC	mg·L <sup>-1</sup>	62.5	36.0
TSS	mg·L <sup>-1</sup>	569.8	231.8
Turbidity	NTU	543.8	230.5

### 2.2. Bench Filtration Unit

The bench filtration unit consisted of a rotating hollow fiber membrane module (R-HFM) vertically immersed in a 3 L tank (15 cm of inner diameter) for performing the direct filtration tests (Figure 1). A ZeeWeed<sup>®</sup> ZW-1 (SUEZ Water Technologies and Solutions, Ontario, ON, Canada) hollow fiber ultrafiltration module of 0.04 µm of pore size with 97 fibers of 1.9 mm outer diameter and 8·10<sup>-2</sup> m of length was used. The module has a nominal membrane surface area of 0.047 m<sup>2</sup>. ZeeWeed<sup>®</sup> consists of a woven reinforcing braid on which a PVDF membrane is casted. Permeate was withdrawn at constant flux (*J*) from the outside to the inside of the fibers by the vacuum created by a magnetic drive gear pump (Micropump-GA Series, AxFlow, Stockholm, Sweden). The system operated in closed loop. The shear rates generated to mitigate membrane fouling were originated by membrane rotation using a mechanical stirrer (Heidolph-RZR2020, Heidolph Instruments GmbH & CO., Schwabach, Germany), which acts as impeller of the R-HFM and is connected to the permeate line.

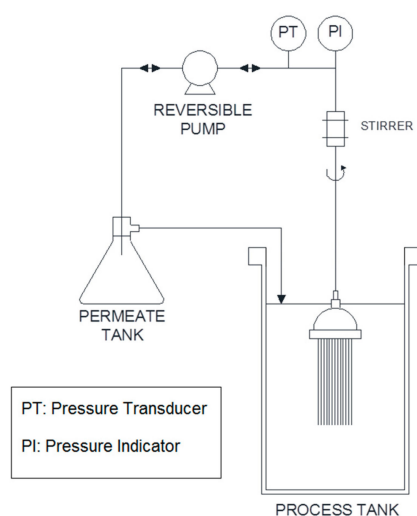


**Figure 1.** Bench filtration unit equipped with the rotating membrane module (R-HFM).

In addition, in order to evaluate membrane fouling and to control the filtration unit, transmembrane pressure (*TMP*) data were registered and acquired by a pressure sensor (Sensotech, Barcelona, Spain)

and the DAQ Factory software (AzeoTech<sup>®</sup>, Inc., Ashland, OR, USA), respectively. The control system also allows setting the main operating variables: the permeate and backwashing fluxes ( $J$  and  $J_B$ , respectively), the filtration and backwashing cycle time ( $t_F$  and  $t_B$ , respectively) and the intermittence operation of the stirrer. A detailed description of the experimental unit can be found in Ruigómez et al. [27].

### 2.3. Flux-Step Assays

The flux-step assays were carried out to evaluate the influence of the rotating speed over membrane fouling. In order to reproduce the operational conditions often employed during the operation, backwashing stages were incorporated after every flux step, modifying the method proposed by Le-Clech et al. [28]. The duration of each step and the flux increment were fixed in 15 min and  $4 \text{ L}\cdot\text{h}^{-1}\cdot\text{m}^{-2}$ , respectively. Between steps, backwashing flux and duration were  $60 \text{ L}\cdot\text{h}^{-1}\cdot\text{m}^{-2}$  and 30 s, respectively. Four different rotating speeds ( $N$ ) were evaluated: 120, 180, 260 and  $340 \text{ rev}\cdot\text{min}^{-1}$ . According to Rector et al. [29], these values generate turbulent flow regimes ( $\text{Re} > 10^4$ ), where the corresponding rotational Reynolds numbers were 13,738; 20,607; 29,766 and 38,924, respectively.

### 2.4. Filtration Tests

Filtration tests were conducted during 30 consecutive filtration/backwashing cycles, where the fouling model parameters were calculated as the average of the last 3 cycles. For each cycle, the filtration and backwashing times were fixed in 450 s and 30 s, respectively. Four permeate fluxes were investigated (4, 12, 16 and  $20 \text{ L}\cdot\text{h}^{-1}\cdot\text{m}^{-2}$ ) with the same backwashing flux of  $60 \text{ L}\cdot\text{h}^{-1}\cdot\text{m}^{-2}$ . All tests were performed with real wastewater at room temperature. The feed concentration was reproducible along the experimental series, showing a low content of solids ( $\text{TSS} = 333 - 870 \text{ mg}\cdot\text{L}^{-1}$ , see Table 1), so feedwater viscosity can be estimated as the natural water one. In addition, transmembrane pressure was continuously registered through the control system ( $\text{TMP} = 2 - 30 \text{ kPa}$ ). Rotation intermittence was evaluated by the dimensionless rotation time ( $\theta$ ), defined as showed in Equation (1):

$$\theta = \frac{(t_{rot})_{on}}{(t_{rot})_{on} + (t_{rot})_{off}} \quad (1)$$

where  $(t_{rot})_{on}$  and  $(t_{rot})_{off}$  are the duration of rotation and non-rotation phases, respectively, during a rotation cycle. For all values,  $(t_{rot})_{on}$  was fixed in 10 s and  $(t_{rot})_{off}$  varied according to the selected  $\theta$  value.

Net rotation speed ( $N_{net}$ ) was defined as the product of the rotation speed and the dimensionless rotation time ( $N_{net} = N\cdot\theta$ ). Two different values were investigated (26 and  $104 \text{ rev}\cdot\text{min}^{-1}$ ) obtained by combining different pairs of  $\theta$  and  $N$  (Table 2).

**Table 2.** Values of  $N$  and  $\theta$  for the selected  $N_{net}$ .

$N_{net} \text{ rev}\cdot\text{min}^{-1}$	$N \text{ rev}\cdot\text{min}^{-1}$	$\theta$
26	30	0.867
26	45	0.578
26	65	0.400
26	85	0.306
104	120	0.867
104	180	0.578
104	260	0.400
104	340	0.306

### 2.5. Membrane Fouling Characterization

Membrane fouling was characterized by a combined model developed for crossflow filtration [30], considering the effect of fouling history on the effective flux [31]. This approach considers three

different mechanisms: residual fouling, intermediate pore blocking and cake filtration. The first one (often named physically irreversible fouling) is caused by adsorption or deposition of fine foulants within the internal membrane structure [25,32] and/or by the formation of a compacted gel/cake under long-term operation [17]. This fouling is expected to produce a reduction in the available membrane surface area and thus to increase the local permeate flux in the unobstructed area. Therefore, an effective permeate flux ( $J_e$ ) can be assumed for considering the effect of fouling history on the filtration performance [31,33]:

$$J_e = J \cdot \frac{TMP_0}{(TMP_0)_{pw}} \quad (2)$$

where  $(TMP_0)_{pw}$  is the transmembrane pressure obtained for pure water (i.e., clean membrane) at  $J$  flux and  $TMP_0$  is the actual transmembrane pressure at the same flux.

During filtration, two fouling mechanisms occur simultaneously. Initially, intermediate pore blocking is the predominant mechanism, evolving over time into a process dominated by cake filtration. During the initial period, the overall hydraulic resistance is assumed to remain constant, since cake layer is negligible. Intermediate pore blocking mechanism considers that foulants have the probability of either to block open pores or to deposit on previously settled foulants, where the rate of pore blocking is proportional to the actual unobstructed membrane surface area. In crossflow filtration, a balance between the pore blocking rate and a foulant removal term (due to shear rate), proportional to the actual obstructed area, is expected. Accordingly,  $TMP$  evolution during this period can be described by Equation (3) [30]:

$$TMP = \frac{TMP_0}{\left(\frac{1}{K_i} + \left(1 - \frac{1}{K_i}\right) \cdot \exp(-K_i \cdot B \cdot t)\right)} \quad (3)$$

where  $K_i$  is the intermediate pore blocking constant,  $B$  is the removal rate constant ( $s^{-1}$ ) and  $t$  is the operation time (s). Likewise,  $K_i$  is related to pore blocking and foulant removal rate constants (Equation (4)):

$$K_i = 1 + \frac{\sigma \cdot J_e}{B} \quad (4)$$

where  $\sigma$  is the blocked membrane area per unit of filtrate volume ( $m^{-1}$ ), and the product  $\sigma \cdot J_e$  can be considered as a pore blocking rate constant.

As filtration proceeds, foulant layers accumulate on the membrane surface, increasing the overall hydraulic resistance. By using the Darcy's Law, Equation (3) can be rewritten to consider the cake filtration mechanism (Equation (5)) [30]:

$$TMP = \frac{TMP_0 \cdot (1 + K_c \cdot J_e \cdot t)}{\left(\frac{1}{K_i} + \left(1 - \frac{1}{K_i}\right) \cdot \exp(-K_i \cdot B \cdot t)\right)} \quad (5)$$

where  $K_c$  is the cake filtration constant ( $m^{-1}$ ) and represents the cake accumulation rate.

## 2.6. Wastewater Fractionation

The feedwater has been segregated in two different samples: supernatant and filtrate ( $\leq 1-3 \mu m$ ). Supernatant was obtained after 2 h of feedwater sedimentation. Filtrate samples were obtained by filtering the supernatant through 1–3  $\mu m$  filter sheets (Seitz® K-100, Pall Corporation, New York, NY, USA). The main properties of each sample are shown in Table 3. Their fouling behavior were evaluated by short-term filtration tests (four consecutive filtration/backwashing cycles). For each sample, the obtained  $TMP$  profiles were fitted to the fouling model. Then, it was assumed that the model parameters for the feedwater can be divided into the relative contribution of three fractions: settling particles, non-settling particles, and colloidal and soluble components. The contribution of the settling particles has been obtained by the subtraction of the feedwater and supernatant model coefficients. Likewise, non-settling particles contribution has been determined by the difference

between the supernatant and the filtrate. The rest constitutes the contribution of the colloidal and soluble fraction.

**Table 3.** Main characteristics of the different fractions of feedwater.

Parameter	Units	Feedwater	Supernatant	Filtrate (<1–3 $\mu\text{m}$ )
COD	$\text{mg}\cdot\text{L}^{-1}$	1176	663	368
DOC	$\text{mg}\cdot\text{L}^{-1}$	114	133	120
TSS	$\text{mg}\cdot\text{L}^{-1}$	457	145	n.d.
Turbidity	NTU	411	153	37

n.d.: not detected.

### 2.7. Analytical Methods

Chemical oxygen demand (COD), dissolved organic carbon (DOC), total suspended solids (TSS) and turbidity were analyzed according to the Standard Methods [34].

## 3. Results and Discussion

### 3.1. Determination of Threshold Fluxes: Effect of Rotation Speed

The determination of the threshold flux and the threshold flux for irreversibility allows to evaluate the fouling development and its irreversibility, and thus, to design an optimal operation strategy (i.e., permeate flux and rotation speed). Given its simplicity, the threshold fluxes are often measured by the improved flux-steps method [35]. Figure 2 shows the typical *TMP* profiles during the flux-step testing. Regarding irreversible fouling, it can be evaluated by analyzing the initial transmembrane pressures ( $TMP_0$ ), obtained after each backwashing step. Increasing flux produced a sharp increase in the  $TMP_0$ , which involves a deviation from the theoretical behavior described by the Darcy's equation for pure water. The existence of the irreversible fouling is also corroborated by the progressive decrease observed in the backwashing *TMP*. Therefore, a threshold flux value for irreversibility ( $(J_{th})_{irr}$ ) can be identified ( $48 \text{ L}\cdot\text{h}^{-1}\cdot\text{m}^{-2}$  in the example), beyond which the backwashing, under given conditions (i.e., backwashing flux, duration and rotation speed), was not capable of completely removing the fouling, as reported for activated sludge and model suspensions [35–37]. This approach is based on the existence of a critical deposited mass, which arises from a balance between convective and back-transport of foulants [38]. According to a combined model (cf. Equation (5)), after the backwashing, fouling is initially governed by pore blocking, transitioning over time to cake filtration [30]. As seen in detail in Figure 2, at fluxes above the threshold, the *TMP* slightly increased until achieving a value related to intermediate pore blocking mechanism ( $TMP_i = K_i \cdot TMP_0$ ) and then linearly rising due to the cake filtration mechanism. Hence, above the threshold value, the latter is the dominant mechanism. It has been reported that the cake layer becomes more compact when filtering at higher fluxes during relative large periods, being more difficult to detach by physical cleanings [39]. In addition, the irreversible fouling layer could decrease the available filtration area during the successive steps, which can justify the sharp increase of  $TMP_0$  observed at fluxes higher than  $(J_{th})_{irr}$  (Figure 2).

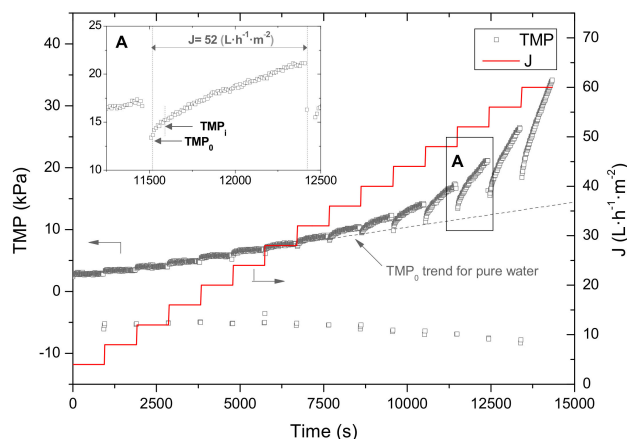


**Figure 2.** Transmembrane pressure (*TMP*) and flux (*J*) profiles during a flux-stepping test.  $N = 340 \text{ rev}\cdot\text{min}^{-1}$ .  $TMP_0$ : initial *TMP* for each step (after backwashing);  $TMP_i$ : asymptotic *TMP* value for intermediate pore blocking mechanism.

Based on the above approach, the same procedure was applied for other rotation speeds ( $N$ ), showing a substantial influence on  $(J_{th})_{irr}$  (Table 4). As expected, increasing the shear by rotation declined the fouling deposition rate (i.e.,  $dTMP/dt$ ) and, in turn, increased the flux required to achieve irreversible fouling. Specifically, varying the rotation speed from 120 to  $340 \text{ rev}\cdot\text{min}^{-1}$  increased the  $(J_{th})_{irr}$  by a factor of 2.4. As seen, the rotation efficiency remained nearly constant during the whole tested range, where a correlation  $(J_{th})_{irr} \sim N^{0.9}$  was found. According to several authors, the shear sensitivity over the operating flux in dynamic filtration can be assessed by the exponent parameter in a power-law function [23,40]. This empirical parameter typically ranges between 0.2 and 1.5, being influenced by feedwater characteristics, membrane type, system configuration and *TMP* applied [23]. Considering the configuration presented in this work as a stirred vessel with the rotating membrane acting as an impeller, the average shear rate in the fluid is function of  $N^{3/2}$  under turbulent regime ( $Re > 10^4$ , cf. Section 2.3) [41]. Accordingly, a power-law exponent of about 0.6 can be assumed, suggesting a shear efficiency comparable with those typically reported for the wide established dynamic filtration modules [24].

**Table 4.** Threshold flux, threshold flux for irreversibility and main model parameters for cake filtration under each rotation speed.

$N$	$J_{th, irr}$	$J_{th}$	$\alpha_c \cdot \omega_c$	$\alpha_{ss} \cdot \omega_{ss}$	$\alpha_{ss} \cdot S$
$\text{rev}\cdot\text{min}^{-1}$	$\text{L}\cdot\text{h}^{-1}\cdot\text{m}^{-2}$	$\text{L}\cdot\text{h}^{-1}\cdot\text{m}^{-2}$	$\text{m}^{-2}$	$\text{m}^{-2}$	$\text{m}^{-1}\cdot\text{s}^{-1}$
120	20	12	$8.6 \times 10^{13}$	$2.2 \times 10^{14}$	$8.2 \times 10^8$
180	24	16	$6.6 \times 10^{13}$	$1.8 \times 10^{14}$	$8.3 \times 10^8$
260	40	28	$1.8 \times 10^{13}$	$9.7 \times 10^{13}$	$7.2 \times 10^8$
340	48	32	$8.3 \times 10^{12}$	$4.0 \times 10^{13}$	$3.4 \times 10^8$

With regard to reversible fouling, the threshold flux ( $J_{th}$ ) ( $32 \text{ L}\cdot\text{h}^{-1}\cdot\text{m}^{-2}$  in Figure 2) has been widely used for discerning regions with different levels of fouling rates [38,42]. At low fluxes, the fouling rates remained at very low values, while at fluxes slightly higher than the threshold, the *TMP* continuously increased during the filtration step but at a rate not high enough to form an irreversible deposit (i.e., critical mass). As a consequence, a flux range can be found between both threshold fluxes (from 32 to  $48 \text{ L}\cdot\text{h}^{-1}\cdot\text{m}^{-2}$  in the example), where the fouling of large particles can be effectively controlled. This range tended to decrease in values and amplitude at lower rotation speeds, due to the similar effectiveness of shear in both fluxes (Table 4). As mentioned before, the observed fouling behavior can be physically interpreted through the combined intermediate pore blocking and cake filtration model (cf. Equation (5)). The two specific model parameters  $K_i$  (pore blocking) and  $K_c$  (cake filtration) can

be calculated by fitting the  $TMP$  trend for each step, where the slope during the linear growth phase should equal  $TMP_0 \cdot K_i \cdot K_c \cdot J_e$ . Figure 3 shows the plots of both parameters against effective permeate flux.  $K_i$  data show a high dispersion without a clear influence of the hydrodynamic conditions. It should be noted that the increase of  $K_i$  over 1 denotes the relationship between the rate constants of pore blocking and its removal. Due to the relative low values, pore blocking seems to have a minor role in the fouling behavior at tested conditions. Conversely, permeate flux and rotation speed governed cake filtration. As seen in Figure 3b, the cake formation rate, expressed as the specific model parameter  $K_c \cdot TMP_0$ , followed the characteristic trend where the threshold flux marked a transition from low to high fouling rates. One can argue, according to others [36,43], that the threshold flux is determined by the deposition of large particles (i.e., suspended solids). It follows, for a polydisperse suspension, that the cake layer is formed by fine particles (i.e., colloids) at low fluxes, while at fluxes beyond the threshold value, large particles determined the cake formation. According to the proposed model,  $K_c \cdot TMP_0$  profile can be described by the following equations:

$$K_c \cdot TMP_0 = \mu \cdot \alpha_c \cdot \omega_c \cdot J_e \quad J_e < J_{th} \quad (6)$$

$$K_c \cdot TMP_0 = \mu \cdot \alpha_c \cdot \omega_c \cdot J_e + \mu \cdot \alpha_{ss} \cdot (\omega_{ss} \cdot J_e - S) \quad J_e > J_{th} \quad (7)$$

where  $\mu$  is the permeate viscosity (Pa·s);  $\alpha_c$  and  $\alpha_{ss}$  are the specific cake resistances ( $\text{m} \cdot \text{kg}^{-1}$ ) for the colloidal and suspended components, respectively;  $\omega_c$  and  $\alpha_{ss}$  are the solid concentrations per unit of filtrate volume ( $\text{kg} \cdot \text{m}^{-3}$ ) for the colloidal and suspended components, respectively, and  $S$  is the cake erosion rate per unit area ( $\text{kg} \cdot \text{m}^{-2} \cdot \text{s}^{-1}$ ).

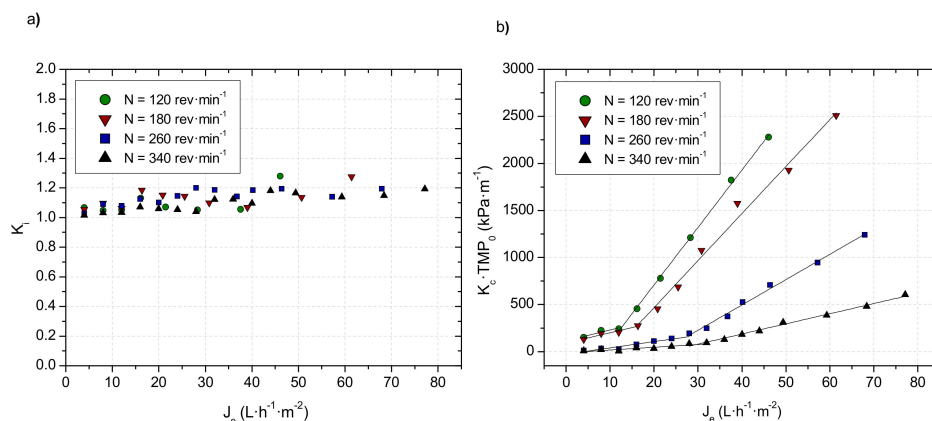


**Figure 3.** Model parameters  $K_i$  (a) and  $K_c \cdot TMP_0$  (b) against effective permeate flux ( $J_e$ ) at different rotation speeds.

Based on the above approach, the threshold flux is governed by a balance between large particle deposition and cake erosion. It has been assumed that the erosion process will only be significant for a cake formed by large particles (i.e., suspended solids), in accordance with previous studies [44]. Therefore, the cake erosion rate can be calculated at each threshold flux (cf. Equation (7)). Main model parameters for cake filtration are shown in Table 4. Interestingly, as  $N$  increased, both  $\alpha_c \cdot \omega_c$  and  $\alpha_{ss} \cdot \omega_{ss}$  decreased in comparable relative values (i.e.,  $\sim 90\%$  and  $\sim 82\%$ , respectively). Hence, the high shear induced by rotation partially mitigated colloids deposition, even though a lower back-transport is recognized for fine particles [45]. On the other hand, cake erosion rate tended to decrease with  $N$ , which can be attributed to the lower deposition rate.

In summary, it may be concluded that the results demonstrated a significant flux improvement; however, it should be noted that the operation at steady rotation speed is energy intensive. For turbulent flow, the power input in stirred tanks is function of  $N^3$  [41], therefore a 2.4-fold improvement would require about 22-fold increase in the power. Furthermore, conducting the operation at high rotation

speed may decrease the fouling removal by cake erosion. Therefore, in the following sections intermittent shear rotation was investigated for reducing the energy demand of the process.

### 3.2. Effect of Rotation Intermittence on Filtration Performance

In order to reproduce typical operation conditions, the fouling tests comprised several consecutive filtration/backwashing cycles (cf. Section 2.4). As an example, Figure 4 shows *TMP* profiles at 0.4 of dimensionless rotation time with a fixed speed of  $260 \text{ rev}\cdot\text{min}^{-1}$  during the rotation periods. In Figure 5, average model parameters at pseudo-stationary conditions are plotted against  $\theta$  for the different sub-threshold fluxes investigated ( $4, 12, 16$  and  $20 \text{ L}\cdot\text{h}^{-1}\cdot\text{m}^{-2}$ ).

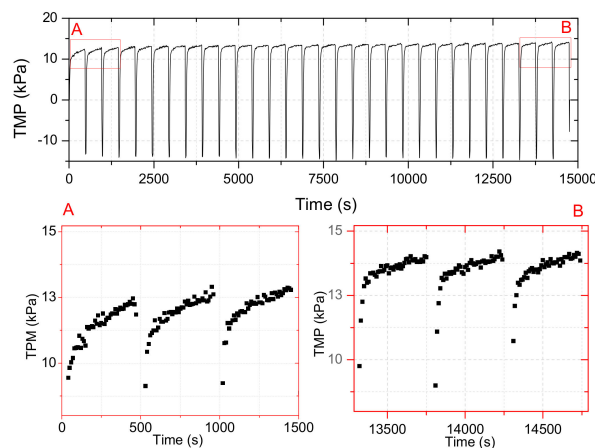


**Figure 4.** *TMP* evolution with consecutive filtration/backwashing cycles.  $J = 16 \text{ L}\cdot\text{h}^{-1}\cdot\text{m}^{-2}$ ;  $N = 260 \text{ rev}\cdot\text{min}^{-1}$ ;  $\theta = 0.4$ . (A) corresponds to the three first cycles while (B) refers to three cycles at pseudo-stationary regime.

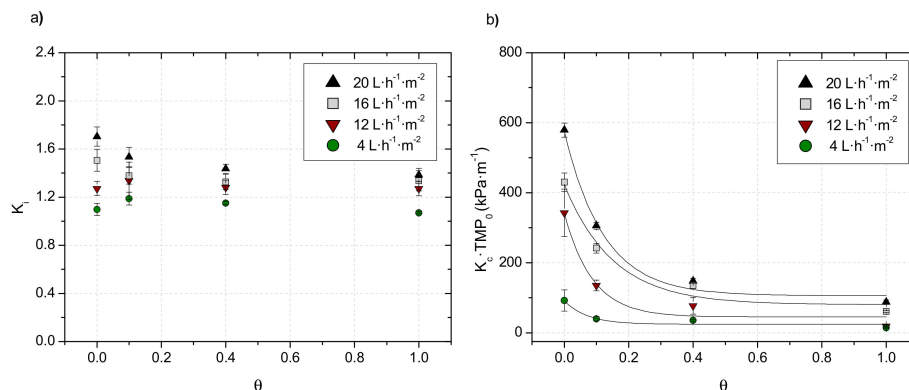


**Figure 5.** Model parameters  $K_i$  (a) and  $K_c \cdot \text{TMP}_0$  (b) against dimensionless rotation time ( $\theta$ ) at different sub-threshold fluxes.  $N = 260 \text{ rev}\cdot\text{min}^{-1}$ .

As seen in Figure 5a,  $K_i$  increased with the permeate flux and slightly decreased with  $\theta$ , which is consistent with the proposed model (Equation (4)). However, it shows that increasing the intermittence of rotation over 0.4 (i.e., 10/15 on/off) has no substantial effect on controlling the pore blocking fouling. By comparing  $K_i$  values with those obtained in the flux-step tests (Figure 3a), this type of fouling tended to increase with the operation time. This can be also observed in Figure 4, where significant changes in the fouling pattern with successive filtration/backwashing cycles were found. As seen, the pore blocking becomes the predominant fouling mechanism at large operation times, which accounted for approximately 80% of the global *TMP* increase (Figure 4, detail B). Furthermore, a transition from this fouling to a residual one (i.e., irreversible) after a long-term operation has been reported [17]. As a consequence, while the pore blocking fouling is expected to be reduced to some extent by optimizing the backwashing conditions [46], the application of frequent chemical cleanings, required to remove

the irreversible fouling, seems to be inherent to the process [10,25]. On the other hand, Figure 5b shows that  $K_c \cdot TMP_0$  decreased exponentially with increasing  $\theta$  in all cases. In this case, values higher than 0.4 did not result in a significant improvement. As seen, the effectiveness of the intermittent rotation increases with flux. Therefore, results revealed that imposing a proper rotation intermittence might significantly reduce energy demand, whilst maintaining a fouling control comparable to that achieved by continuous rotation.

### 3.3. Influence of the Net Rotation Speed

In previous sections, the impact of the rotation speed and the rotation intermittence on membrane fouling has been examined in terms of the combined model coefficients. However, their relationship is of great practical interest in order to optimize operating conditions and, consequently, the energy consumption. Since power is proportional to membrane motion and rotation depends on the  $N$  and  $\theta$  values, the product between both parameters has been defined as the net rotation speed ( $N_{net} = N \cdot \theta$ ). Based on the previous section, very low  $\theta$  values were avoided due to the lesser fouling control. Figure 6 shows  $K_i$  and  $TMP_0 \cdot K_c$  against  $N$  for two different  $N_{net}$  values (26 and 104  $\text{rev} \cdot \text{min}^{-1}$ ) obtained by combining different pairs of  $\theta$  (from 0.31 to 0.87) and  $N$  (from 30 to 340  $\text{rev} \cdot \text{min}^{-1}$ ) (cf. Section 2.4). All tests were performed at  $J$  of 20  $\text{L} \cdot \text{h}^{-1} \cdot \text{m}^{-2}$  and the same backwashing conditions described above.

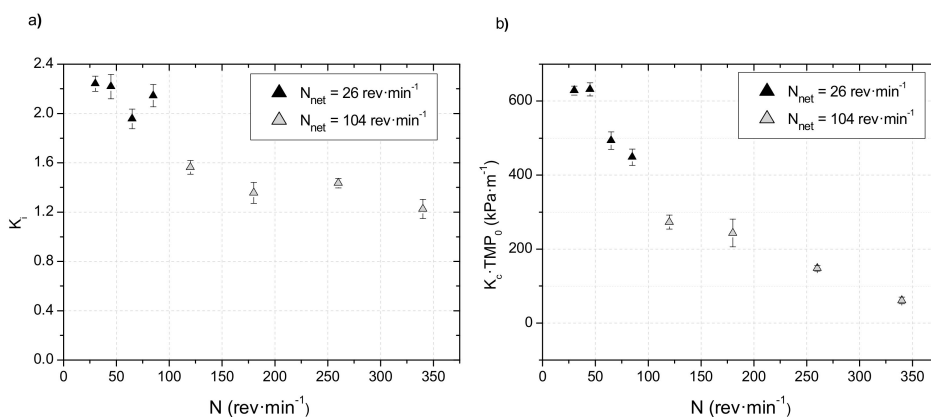


**Figure 6.** (a)  $K_i$  and (b)  $TMP_0 \cdot K_c$  against rotation speed ( $N$ ) for two different  $N_{net}$  values: 26 and 104  $\text{rev} \cdot \text{min}^{-1}$ .  $J = 20 \text{ L} \cdot \text{h}^{-1} \cdot \text{m}^{-2}$ .

$K_i$  at pseudo-stationary conditions under different  $N$  values is shown in Figure 6a. The results indicate that the pore blocking coefficient decreases exponentially with the rotation speed applied during the rotation periods. Consequently, a plateau was observed in the range of 1.2–1.4, when  $N$  was equal or higher than 180  $\text{rev} \cdot \text{min}^{-1}$ . Results also suggest that there was a low-turbulence region ( $N \leq 45 \text{ rev} \cdot \text{min}^{-1}$ ;  $\text{Re} \leq 5152$ ) where the shear rates are too weak to control pore blocking. In agreement with a recent work, the reason of this trend may be related to the deposition of micron and submicron-size particles on the membrane surface, which could not be mitigated operating at low shear rates [27]. On the other hand, Figure 6b shows  $K_c \cdot TMP_0$  profiles against  $N$ , where the values remained approximately constant at  $\sim 630 \text{ kPa} \cdot \text{m}^{-1}$  until the rotation speed reached the turning point. Then, a decreasing trend in fouling with the increase of the rotation speed can be observed. Therefore, for a given energy demand, the optimal operating conditions involve large speeds with low to moderate dimensional rotation times ( $\sim 0.3$ – $0.4$ ). Although the optimal speed value depends on the module design, the system hydrodynamics and the operating conditions; its identification is a key factor to enhance process sustainability in terms of energy consumption.

### 3.4. Fouling Fractions Contribution

In order to assess a deeper analysis of the fouling mechanisms involved, the wastewater was separated in the three main fractions (settling particles, non-settling particles and colloidal and soluble

matter) and filtered at different  $\theta$  values (0.1, 0.4 and 1). Figure 7 displays the relative contribution of fractions to the total value of  $K_i$  (Figure 7a) and  $TMP_0 \cdot K_c$  (Figure 7b), which were obtained as the average values of the first four filtration cycles. The assays were performed at  $260 \text{ rev} \cdot \text{min}^{-1}$  during the rotation periods and with a permeate flux of  $20 \text{ L} \cdot \text{h}^{-1} \cdot \text{m}^{-2}$ .

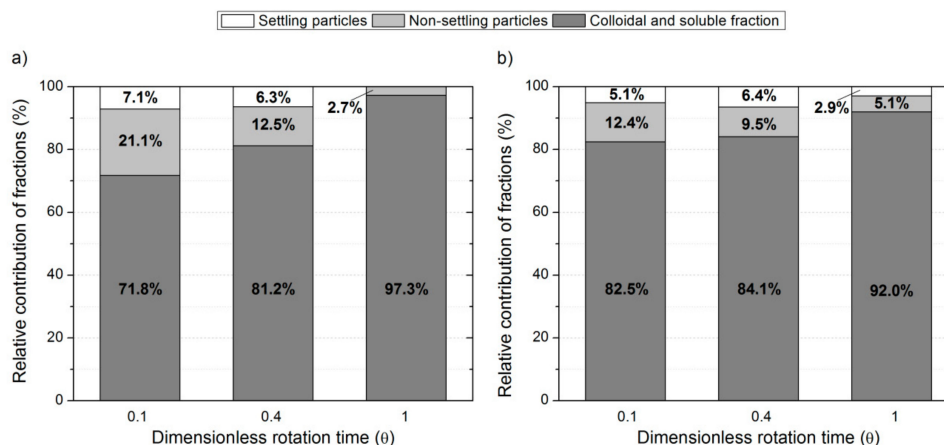


**Figure 7.** Relative contribution of fractions to (a)  $K_i$  and (b)  $TMP_0 \cdot K_c$  against dimensionless rotation time ( $\theta$ ).  $N = 260 \text{ rev} \cdot \text{min}^{-1}$ ;  $J = 20 \text{ L} \cdot \text{h}^{-1} \cdot \text{m}^{-2}$ .

Figure 7a shows a progressive decrease of  $K_i$  with  $\theta$  for all fractions, where the colloidal and soluble fraction ( $\leq 1\text{--}3 \mu\text{m}$ ) was the main contribution, increasing its relative value with the dimensionless rotation time, from 71.8% ( $\theta = 0.1$ ) to 97.3% ( $\theta = 1$ ). As mentioned before, it was assumed that the fouling at fluxes below the threshold value was caused by fine particles (i.e., colloids), which is consistent with the presented results. This behavior confirms that the shear efforts generated by rotation cannot effectively control the progressive accumulation of fine foulants in the membrane vicinity causing a pore blocking fouling. Nevertheless, the settling particles hardly contribute to the total value of  $K_i$  (0–7.1%), and the non-settling particles percentage decreased down to 2.7% when  $\theta = 1$ .

As expected, a similar trend was observed for the product  $TMP_0 \cdot K_c$  (Figure 7b). Results show a decrease of the colloidal and soluble fraction contribution from 92.0% to 82.5% when  $\theta$  was reduced from 1 to 0.1, respectively. Simultaneously, the non-settling particles percentage increased from 5.1% to 12.4%, while that related to settling particles remained approximately constant. According to previous studies, large particles could be easily removed from the membrane surface by erosion phenomena [47]. These results are consistent with the findings reported by Ji et al., during the evaluation of a dynamic crossflow filtration system with a rotating tubular membrane using hollow glass microspheres as model particles [44]. The authors found that the shear rates generated by the rotation-induced centripetal force preferentially dislodge large particles ( $>5\text{--}10 \mu\text{m}$ ) from the cake.

In summary, results show the high effectiveness of membrane rotation in the control of fouling related to large particles, even at low  $\theta$  values. Nevertheless, cake consolidation due to the substantial residual fouling caused by fine foulants would be expected at high operational times. Thus, it would be useful to carry out future long-term pilot-scale researches in order to improve the knowledge of fouling phenomena during direct membrane filtration processes.

#### 4. Conclusions

The influence of rotation speed, intermittence and permeate flux has been studied in a rotating hollow fiber module applied to direct membrane filtration of wastewater. The filtration performance has been evaluated by using a fouling model combining residual fouling, intermediate pore blocking and cake filtration. From this work, the following may be concluded:

- Membrane rotation has demonstrated a significant threshold flux improvement, where a correlation  $(J_{th})_{irr} \sim N^{0.9}$  has been found. Fouling behavior can be well described by the combined model, where a balance between large particle deposition and cake erosion governs the threshold flux.
- At fluxes below the threshold, pore blocking becomes the predominant fouling mechanism at large operation times. In these conditions, proper rotation intermittence (10/15 on/off) might significantly reduce energy demand, whilst maintaining a fouling control comparable to that achieved for the continuous rotation.
- Rotation intermittence plays a significantly minor role than rotation speed on membrane fouling mitigation. Therefore, for a given energy demand, the optimal operating conditions involve high speeds with low to moderate intermittences.
- At sub-threshold fluxes, membrane rotation demonstrated its high effectiveness in preventing fouling phenomena linked to large particles (settling and non-settling ones). Therefore, colloidal and macromolecules have been found as the main contribution to membrane fouling.

**Author Contributions:** Conceptualization, I.R. and L.V.; methodology, I.R.; software, I.R.; validation, I.R. and L.R.-G.; formal analysis, I.R. and E.G.; investigation, I.R.; resources, L.V.; data curation, E.G.; writing—original draft preparation, I.R.; writing—review and editing, E.G. and L.R.-G.; supervision, L.V.; project administration, L.V.; funding acquisition, L.V. All authors have read and agreed to the published version of the manuscript.

**Funding:** This research was funded by Fundación CajaCanarias and Fundación Bancaria La Caixa-convocatoria 2017 grant number 2017REC25.

**Acknowledgments:** This work is framed within the research project 2017REC25 “Regeneración de espacios marinos y costeros de Canarias aplicando filtración por membranas a las aguas residuales”, which is developed with the financial support of Fundación CajaCanarias and Fundación Bancaria La Caixa-convocatoria 2017. The authors wish to express their gratitude to Tenerife Water Council (CIATF) and SACYR for supplying primary effluent. Likewise, the authors are grateful to the Water Analysis Laboratory of the ULL Chemical Engineering Department and the Research Support General Service (SEGAI) of ULL for the analytical support.

**Conflicts of Interest:** The authors declare no conflict of interest.

## References

1. UN. *Sustainable Development Goal 6 Synthesis Report 2018 on Water and Sanitation*; UN: New York, NY, USA, 2018.
2. Voulvoulis, N. Water reuse from a circular economy perspective and potential risks from an unregulated approach. *Curr. Opin. Environ. Sci. Health* **2018**, *2*, 32–45. [[CrossRef](#)]
3. USEPA (US Environmental Protection Agency). *Guidelines for Water Reuse*; USEPA: Anchorage, AK, USA, 2012.
4. Amec, F.W.; IEEP; ACTeon; IMDEA; NTUA. *EU-Level Instruments on Water Reuse*; Publications Office of the EU: Brussels, Belgium, 2016.
5. WWAP (United Nations World Water Assessment Programme). *The United Nations World Water Development Report 2017; Wastewater, The Untapped Resource*; United Nations: Paris, France, 2017.
6. Asano, T.; Burton, F.L.; Leverenz, H.L.; Tsuchihashi, R.; Tchobanoglous, G. *Water Reuse, Issues, Technologies, and Applications*; McGraw-Hill: New York, NY, USA, 2007.
7. Hube, S.; Eskafi, M.; Hrafnkelsdóttir, K.F.; Bjarnadóttir, B.; Bjarnadóttir, M.Á.; Axelsdóttir, S.; Wu, B. Direct membrane filtration for wastewater treatment and resource recovery: A review. *Sci. Total Environ.* **2020**, *710*, 136375. [[CrossRef](#)] [[PubMed](#)]
8. Nascimento, T.A.; Fdz-Polanco, F.; Peña, M. Membrane-Based Technologies for the Up-Concentration of Municipal Wastewater: A Review of Pretreatment Intensification. *Sep. Purif. Rev.* **2020**, *49*, 1–19. [[CrossRef](#)]
9. Nascimento, T.A.; Mejía, F.R.; Fdz-Polanco, F.; Peña Miranda, M. Improvement of municipal wastewater pretreatment by direct membrane filtration. *Environ. Technol.* **2017**, *38*, 2562–2572. [[CrossRef](#)]
10. Lateef, S.K.; Soh, B.Z.; Kimura, K. Direct membrane filtration of municipal wastewater with chemically enhanced backwash for recovery of organic matter. *Bioresour. Technol.* **2013**, *150*, 149–155. [[CrossRef](#)]
11. Kramer, F.C.; Shang, R.; Heijman, S.G.J.; Scherrenberg, S.M.; Van Lier, J.B.; Rietveld, L.C. Direct water reclamation from sewage using ceramic tight ultra- and nanofiltration. *Sep. Purif. Technol.* **2015**, *147*, 329–336. [[CrossRef](#)]

12. Lin, H.; Zhang, M.; Wang, F.; Meng, F.; Liao, B.Q.; Hong, H.; Chen, J.; Gao, W. A critical review of extracellular polymeric substances (EPSs) in membrane bioreactors: Characteristics, roles in membrane fouling and control strategies. *J. Memb. Sci.* **2014**, *460*, 110–125. [[CrossRef](#)]
13. Wang, R.; Liang, D.; Liu, X.; Fan, W.; Meng, S.; Cai, W. Effect of magnesium ion on polysaccharide fouling. *Chem. Eng. J.* **2020**. [[CrossRef](#)]
14. Meng, S.; Meng, X.; Fan, W.; Liang, D.; Wang, L.; Zhang, W.; Liu, Y. The role of transparent exopolymer particles (TEP) in membrane fouling: A critical review. *Water Res.* **2020**, *22*, 485–497. [[CrossRef](#)]
15. Yoon, S.H. *Membrane Bioreactor Processes: Principles and Applications*; CRC Press: Boca Raton, FL, USA, 2015.
16. Diamantis, V.I.; Antoniou, I.; Athanasoulia, E.; Melidis, P.; Aivasidis, A. Recovery of reusable water from sewage using aerated flat-sheet membranes. *Water Sci. Technol.* **2010**, *62*, 2769–2775. [[CrossRef](#)]
17. Zhao, Y.; Li, P.; Li, R.; Li, X. Direct filtration for the treatment of the coagulated domestic sewage using flat-sheet ceramic membranes. *Chemosphere* **2019**, *223*, 383–390. [[CrossRef](#)] [[PubMed](#)]
18. Zhou, W.; Wang, J.; Chen, P.; Ji, C.; Kang, Q.; Lu, B.; Li, K.; Liu, J.; Ruan, R. Bio-mitigation of carbon dioxide using microalgal systems: Advances and perspectives. *Renew. Sustain. Energy Rev.* **2017**, *76*, 1163–1175. [[CrossRef](#)]
19. Huang, B.C.; Guan, Y.F.; Chen, W.; Yu, H.Q. Membrane fouling characteristics and mitigation in a coagulation-assisted microfiltration process for municipal wastewater pretreatment. *Water Res.* **2017**, *123*, 216–223. [[CrossRef](#)]
20. Jin, Z.; Meng, F.; Gong, H.; Wang, C.; Wang, K. Improved low-carbon-consuming fouling control in long-term membrane-based sewage pre-concentration: The role of enhanced coagulation process and air backflushing in sustainable sewage treatment. *J. Memb. Sci.* **2017**, *529*, 252–262. [[CrossRef](#)]
21. Choo, K.H.; Choi, S.J.; Hwang, E.D. Effect of coagulant types on textile wastewater reclamation in a combined coagulation/ultrafiltration system. *Desalination* **2007**, *202*, 262–270. [[CrossRef](#)]
22. Cui, X.; Zhou, D.; Fan, W.; Huo, M.; Crittenden, J.C.; Yu, Z.; Ju, P.; Wang, Y. The effectiveness of coagulation for water reclamation from a wastewater treatment plant that has a long hydraulic and sludge retention times: A case study. *Chemosphere* **2016**, *157*, 224–231. [[CrossRef](#)]
23. Zsirai, T.; Qiblawey, H.; A-Marri, M.J.; Judd, S. The impact of mechanical shear on membrane flux and energy demand. *J. Memb. Sci.* **2016**, *516*, 56–63. [[CrossRef](#)]
24. Jaffrin, M.Y. Dynamic filtration with rotating disks, and rotating and vibrating membranes: An update. *Curr. Opin. Chem. Eng.* **2012**, *1*, 171–177. [[CrossRef](#)]
25. Kimura, K.; Honoki, D.; Sato, T. Effective physical cleaning and adequate membrane flux for direct membrane filtration (DMF) of municipal wastewater: Up-concentration of organic matter for efficient energy recovery. *Sep. Purif. Technol.* **2017**, *181*, 37–43. [[CrossRef](#)]
26. Mezohegyi, G.; Bilad, M.R.; Vankelecom, I.F.J. Direct sewage up-concentration by submerged aerated and vibrated membranes. *Bioresour. Technol.* **2012**, *118*, 1–7. [[CrossRef](#)]
27. Ruigómez, I.; González, E.; Galán, P.; Rodríguez-Sevilla, J.; Vera, L. A Rotating Hollow Fiber Module for Fouling Control in Direct Membrane Filtration of Primary Settled Wastewater. *Ind. Eng. Chem. Res.* **2019**, *58*, 16901–16910. [[CrossRef](#)]
28. Le Clech, P.; Jefferson, B.; Chang, I.S.; Judd, S.J. Critical flux determination by the flux-step method in a submerged membrane bioreactor. *J. Memb. Sci.* **2003**, *227*, 81–93. [[CrossRef](#)]
29. Rector, T.J.; Garland, J.L.; Starr, S.O. Dispersion characteristics of a rotating hollow fiber membrane bioreactor: Effects of module packing density and rotational frequency. *J. Memb. Sci.* **2006**, *278*, 144–150. [[CrossRef](#)]
30. Kirschner, A.Y.; Cheng, Y.H.; Paul, D.R.; Field, R.W.; Freeman, B.D. Fouling mechanisms in constant flux crossflow ultrafiltration. *J. Memb. Sci.* **2019**. [[CrossRef](#)]
31. Ognier, S.; Wisniewski, C.; Grasmick, a. Membrane bioreactor fouling in sub-critical filtration conditions: A local critical flux concept. *J. Memb. Sci.* **2004**, *229*, 171–177. [[CrossRef](#)]
32. Zhao, Y.X.; Li, P.; Li, R.H.; Li, X.Y. Characterization and mitigation of the fouling of flat-sheet ceramic membranes for direct filtration of the coagulated domestic wastewater. *J. Hazard. Mater.* **2020**, *385*, 121557. [[CrossRef](#)]
33. Lodge, B.; Judd, S.J.; Smith, A.J. Characterisation of dead-end ultrafiltration of biotreated domestic wastewater. *J. Memb. Sci.* **2004**, *231*, 91–98. [[CrossRef](#)]
34. APHA. *Standard Methods for the Examination of Water and Wastewater*, 21st ed.; American Public Health Association: Washington, DC, USA, 2005.

35. Martí-Calatayud, M.C.; Schneider, S.; Yüce, S.; Wessling, M. Interplay between physical cleaning, membrane pore size and fluid rheology during the evolution of fouling in membrane bioreactors. *Water Res.* **2018**, *147*, 393–402. [[CrossRef](#)]
36. Diez, V.; Ezquerro, D.; Cabezas, J.L.; García, A.; Ramos, C. A modified method for evaluation of critical flux, fouling rate and in situ determination of resistance and compressibility in MBR under different fouling conditions. *J. Memb. Sci.* **2014**, *453*, 1–11. [[CrossRef](#)]
37. Van der Marel, P.; Zwijnenburg, A.; Kemperman, A.; Wessling, M.; Temmink, H.; van der Meer, W. An improved flux-step method to determine the critical flux and the critical flux for irreversibility in a membrane bioreactor. *J. Memb. Sci.* **2009**, *332*, 24–29. [[CrossRef](#)]
38. Bacchin, P.; Aïmar, P.; Field, R.W. Critical and sustainable fluxes: Theory, experiments and applications. *J. Memb. Sci.* **2006**, *281*, 42–69. [[CrossRef](#)]
39. Ye, Y.; Chen, V.; Le-Clech, P. Evolution of fouling deposition and removal on hollow fibre membrane during filtration with periodical backwash. *Desalination* **2011**, *283*, 198–205. [[CrossRef](#)]
40. Jaffrin, M.Y. Dynamic shear-enhanced membrane filtration: A review of rotating disks, rotating membranes and vibrating systems. *J. Memb. Sci.* **2008**, *324*, 7–25. [[CrossRef](#)]
41. Sánchez Pérez, J.A.; Rodríguez Porcel, E.M.; Casas López, J.L.; Fernández Sevilla, J.M.; Chisti, Y. Shear rate in stirred tank and bubble column bioreactors. *Chem. Eng. J.* **2006**, *124*, 1–5. [[CrossRef](#)]
42. Hughes, D.; Field, R.W. Crossflow filtration of washed and unwashed yeast suspensions at constant shear under nominally sub-critical conditions. *J. Memb. Sci.* **2006**, *280*, 89–98. [[CrossRef](#)]
43. Field, R.W.; Pearce, G.K. Critical, sustainable and threshold fluxes for membrane filtration with water industry applications. *Adv. Colloid Interface Sci.* **2011**, *164*, 38–44. [[CrossRef](#)]
44. Ji, P.; Motin, A.; Shan, W.; Bénard, A.; Bruening, M.L.; Tarabara, V.V. Dynamic crossflow filtration with a rotating tubular membrane: Using centripetal force to decrease fouling by buoyant particles. *Chem. Eng. Res. Des.* **2016**, *106*, 101–114. [[CrossRef](#)]
45. Chew, J.W.; Kilduff, J.; Belfort, G. The behavior of suspensions and macromolecular solutions in crossflow microfiltration: An update. *J. Memb. Sci.* **2020**, *601*, 117865. [[CrossRef](#)]
46. Delgado, S.; Vera, L.; González, E.; Martínez, M.; Vera, L.M.; Bravo, L.R. Effect of previous coagulation in direct ultrafiltration of primary settled municipal wastewater. *Desalination* **2012**, *304*, 41–48. [[CrossRef](#)]
47. Christensen, M.L.; Niessen, W.; Sørensen, N.B.; Hansen, S.H.; Jørgensen, M.K.; Nielsen, P.H. Sludge fractionation as a method to study and predict fouling in MBR systems. *Sep. Purif. Technol.* **2018**, *194*, 329–337. [[CrossRef](#)]



© 2020 by the authors. Licensee MDPI, Basel, Switzerland. This article is an open access article distributed under the terms and conditions of the Creative Commons Attribution (CC BY) license (<http://creativecommons.org/licenses/by/4.0/>).